Thermodynamics of diopside-jadeite

Thermodynamics of mixing in diopside-jadeite, CaMgSi$_2$O$_6$-NaAlSi$_2$O$_6$, solid solution from static lattice energy calculations

Victor L. Vinograd,[1],* Julian.D. Gale[2] and Björn Winkler[1]

[1]*University of Frankfurt, Institute of Geosciences, Senckenberanlage 30, 60054 Frankfurt a.M., Germany*

[2]*Nanochemistry Research Institute, Department of Applied Chemistry, Curtin University of Technology, PO Box U1987, Perth 6845, Western Australia*

Abstract

Static lattice energy calculations (SLEC), based on empirical interatomic potentials have been performed for a set of 800 different structures in 2x2x4 supercell of *C*2/*c* diopside with compositions between diopside and jadeite, and with different states of order of the exchangeable Na/Ca and Mg/Al cations. Excess static energies of these structures have been cluster expanded in a basis set of 37 pair-interaction parameters. These parameters have been used to constrain Monte Carlo simulations of temperature-dependent properties in the range of 273–2023 K and to calculate a temperature-composition phase diagram.

Keywords: Diopside-jadeite solid solution, atomistic simulations, activity-composition relations

* Corresponding author. Tel. +49 69 798 22104

E-mail address: v.vinograd@kristall.uni-frankfurt.de

Introduction

The solid solution between augite, $Ca(MgFe)Si_2O_6$ and jadeite, $NaAlSi_2O_6$, plays an important role in petrology of crustal metamorphic rocks that have experienced high pressures and medium-high temperatures, such as blue schists and eclogies. The minimum pressure of crystallization can be estimated from the mole fraction of the jadeite component in clinopyroxene coexisting with quartz and feldspar (Wood et al., 1980). Besides its practical importance, the solid solution attracts much interest of theoreticians as a typical example of coupled substitution. Ca^{2+} and Mg^{2+}, which occupy M1 and M2 sites in $C2/c$ diopside, are substituted with Na^+ and Al^{3+}, respectively, in jadeite. The peculiar property of the system is a combination of the effects of ordering and exsolution. At temperatures above 600 °C diopside and jadeite are fully miscible within the disordered $C2/c$ phase. At lower temperatures two miscibility gaps develop at Ca- and Na-rich compositions due to the stabilization of the ordered intermediate $P2/n$ phase, omphacite (Carpenter, 1981). The mixing between diopside, $CaMgSi_2O_6$, and jadeite, $NaAlSi_2O_6$, within the disordered $C2/c$ phase has been studied both by calorimetry (Wood et al., 1980) and phase-equilibrium method (Kushiro, 1969; Holland, 1983; Gasparick, 1985). The measured enthalpies of mixing and the activities of the jadeite component have been used as constraints in various phenomenological models, which have permitted extrapolating the mixing properties to a wide temperature interval (Ganguly, 1973; Gasparik, 1985; Cohen and Burnham, 1986; Davidson and Burton, 1987; Carpenter et al., 1990; Holland and Powell, 1996, Nakamura and Banno, 1997, Vinograd, 2002). The cation ordering, which is responsible for the stabilization of the intermediate compound, has been studied extensively as functions of both the temperature and composition (Rossi et al. 1983; Carpenter et al. 1990; Boffa Ballaran et al., 1998). It has been

shown that Mg and Al in the M2 site are ordered stronger than Ca and Na in the M1 site. In the

most ordered samples the fractions of Mg in M22 and M21 sub-sites approach zero and one,

respectively, while the fractions of Ca in M12 and M11 sub-sites approach 0.75 and 0.25. Nearly

all studied samples closely follow the linear relationship $Q_{M2} = 2Q_{M1}$ between the order

parameters. The order parameters are related to the site fractions of Ca or Mg in the sub-sites as

follows

$$Q_{M1} = \frac{P_{Ca}^{M11} - P_{Ca}^{M12}}{P_{Ca}^{M11} + P_{Ca}^{M12}} \quad , \quad Q_{M2} = \frac{P_{Mg}^{M21} - P_{Mg}^{M22}}{P_{Mg}^{M21} + P_{Mg}^{M22}} . \qquad (1)$$

The observed relationship between the order parameters has opened an ongoing speculation on

the ground state structure of omphacite. Rossi et al (1983) suggested that the ground state

corresponds to $Q_{M2} = 1$ and $Q_{M1} = 0.5$. The "half-ordering" of Ca and Na in the M1 site was

argued to give the best local charge balance for the oxygen atoms adjacent to M1. However, this

peculiar ordering scheme has not been yet reproduced in simulation studies. Statistical-

thermodynamic models of Burton and Davidson (1988) and Vinograd (2002) predicted a fully

ordered ground state with $Q_{M2} = Q_{M2} = 1$.

   Although the mixing and ordering effects in the system are well understood on a macroscopic

level, there remains a need for a model, which could relate the macroscopic effects to specific

atomic interactions within the structure of clinopyroxene. Such a model should be robust enough

to reproduce the experimentally observed relationship between Q_{M1} and Q_{M2} parameters.

Particularly instructive would be the understanding of the relationship between the ordering,

exsolution and the substitution mechanism. Here we show that static lattice energy calculations

(SLEC) constrained with unit-cell parameters, atomic coordinates and elastic stiffness constants

of diopside, jadeite and some other pure phases in the Ca-Na-Mg-Al-Si-O system and Monte

Carlo simulations based on the SLEC results permit a near quantitative description of the

experimental facts.

The simulation procedure

Recent developments in solid solution theory and in methods of computer simulations of crystalline compounds make it possible to predict mixing properties and phase diagrams of binary solid solutions as functions of interatomic potentials (e.g. Becker et al. 2000; Bosenick et al. 2001a; Warren et al. 2001; Lavrentiev et al., 2006; Vinograd et al., 2007a). The interatomic potentials for oxides and silicates are usually obtained by fitting to structure and elasticity data on minerals of fixed composition using the software such as GULP (Gale, 1996, 1997; Gale and Rohl, 2003). The modeling of solid solutions requires being able to simulate properties of phases characterized with fractional occupancies. In principle, it is possible to describe such phases using the concept of "virtual atoms" and "mixed potentials" (e.g. Winkler et al. 1991; Bosenick et al., 2001b). Many macroscopic properties of solid solutions such as lattice parameters and bulk moduli can be accurately predicted. However, the mixing properties, such as the excess enthalpy, cannot be modeled well with the "virtual atom model". The problem is that this model places the virtual atom in the average position of the crystal structure and, thus, the substitution effect corresponds to homogeneous deformations of the lattices of the end-members. The model, thus, has no means to take structural relaxations into account. On the contrary, real atoms have numerous possibilities to accommodate to the host lattice via local changes in bond distances and angles. The only possibility to take relaxation effects into account is to work with supercells, where the exchangeable atoms are allowed to shift from the ideal (average) positions. The solid solution can thus be visualized as an immense number of different arrangements of the exchangeable atoms within the supercell. The main breakthrough in the solid solution theory was the understanding that the average thermodynamic properties of the supercell can be well modeled by calculating the energies of a small subset of the possible configurations. The energies

of the other possible arrangements can be accurately predicted with the procedure known as the cluster expansion (Connolly and Williams, 1983; Sanchez et al., 1984). The possibility of an easy and fast evaluation of the energy of any possible configuration within the supercell allows one to apply Monte Carlo method for the calculation of mixing properties.

The empirical potentials

Empirical interatomic potentials allow establishing a link between the structure, elasticity and the static lattice energy of a compound (e.g. Dove, 1993). The force field model of Sanders et al. (1984), which assumes formal charges on cations and anions and involves two-parameter Metal-Oxygen (M-O) Buckingham potentials, three-body O-M-O angle-bending terms and the shell model for the oxygen polarizability, is found to be the most successful for the description of ordering in aluminosilicates (Winkler et al., 1991; Patel et al., 1991; Sainz-Diaz et al., 2001; Bosenick et al., 2001a). Vinograd et al. (2004, 2006) have argued that an even better transferability of the potentials within oxide and silicate structures of variable density can be achieved by multiplying the formal cation and anion charges by the common factor 0.85. The set of potentials for Mg, Al, Si and O, which is used here, has been already tested in the recent simulation study of Vinograd et al. (2007b). This set gives a reasonably good fit to the structure and elasticity data on α-quartz, coesite, stishovite, corundum, the three Al_2SiO_5 polymorphs and Mg-cordierite. The Buckingham Ca-O and Na-O potentials have been developed here using the relax-fitting procedure (Gale 1996) as implemented in the GULP program (Gale 1997; Gale and Rohl, 2003). The Ca-O potential was fitted to structural parameters and elastic stiffness coefficients of diopside, anorthite, grossular and gehlenite. The Na-O potential was fitted to the unit-cell parameters, atomic coordinates and elastic stiffness coefficients of low albite and jadeite. The structural parameters of anorthite and grossular have been taken from Angel et al.

(1990) (sample from Somma) and Rodehorst et al. (2002) (synthetic sample, $T = 156$ K), respectively. The structural parameters of diopside and jadeite were taken from Cameron et al. (1973), while those of gehlenite and low albite were taken from Swainson et al. (1992) and Harlow and Brown (1980), respectively. The elastic stiffness constants of all these phases were taken from the compilation of Bass (1995). In Table 1 and 2 we compare the predicted structural parameters and elastic stiffness coefficients of diopside and jadeite with the available experimental data.

The static lattice energy calculations

The fully relaxed SLEC calculations have been performed at zero K and zero pressure with GULP in the 2x2x4 supercell of $C2/c$ diopside containing 128 exchangeable atoms on a set of randomly modified structures (configurations) with $x=0$ (1), $x =0.125$ (100), $x =0.25$ (100) $x =0.375$ (100), $x =0.5$ (200), $x =0.625$ (100), $x =0.75$ (100), $x =0.875$ (100), and $x =1$ (1) compositions. The numbers of the sampled structures with the same composition are given in parentheses. The initial structures were prepared from the structure of fully ordered omphacite by substituting appropriate numbers of Ca, Mg with Na, Al or vise verse. The excess energies were calculated by subtracting the weighted sum of the energies of diopside and jadeite (Figure 1).

Cluster expansion of the SLEC results

The cluster expansion procedure permits finding a simple equation, which fits the energies of all simulated configurations and, hopefully, predicts the energy of any other possible configuration. Connolly and Williams (1982) and Sanchez (1984) have shown that the excess energy of a configuration can be expanded in terms of energies a hierarchy of clusters, where a cluster is a structurally distinct group of lattice points. A convenient form for such an expansion is known as

the Js formalism (e.g., Bosenick et al., 2001)

$$E_i \approx 1/2 \sum_n z_n P_{AB}^{(n)} J_n + E_0 \tag{2}$$

where z_n, $P_{AB}^{(n)}$, and J_n are the coordination numbers, fractions of AB-type pairs and effective

cluster interactions for pairs of the order n. J_n corresponds to the energy of the exchange reaction

AA + BB = 2AB between atoms A (Ca or Mg) and B (Na or Al) located at the n-th distance. E_0 is

a composition-dependent term, which absorbs contributions to the excess energy not included in

the Js sum. Vinograd and Sluiter (2006) have argued that in systems with size mismatch, such as

pyrope-grossular garnets, E_0 absorbs the effect of strain related to deformation of the end-

members in the process of mixing. Ferreira et al. (1988) have shown that this strain achieves

maximum at an intermediate composition, while the variation of the strain energy with the

composition can be closely described with the equation

$$E_0 = x_1 x_2 (x_1 A_{12} + x_2 A_{21}) \tag{3}$$

where x_1 and x_2 are the mole fractions of the components. Vinograd (2002) have shown that in

the case when the strain energies of the end-members can be approximated with quadratic

functions of the volume change, the values of A_{12} and A_{21} are determined by the square of the

volume difference and the bulk modules of the end-members. Since the volumes of diopside and

jadeite differ significantly, we retain this term in the model. In contrast to the pyrope-grossular

system, the mixing in the diopside-jadeite solid solutions occurs on two sites, therefore, the

interactions split in the three types: the intra-site (M1-M1) Ca-Na interactions, the intra-site (M2-

M2) Mg-Al interactions and the inter-site M1-M2 interactions. These interactions correspond to

the three ordering reactions:

Ca-Ca + Na-Na = Ca-Na + Na-Ca.,

Mg-Mg + Al-Al = Mg-Al + Al-Mg,

and

Ca-Mg + Na-Al = Ca-Al + Na-Mg.
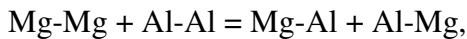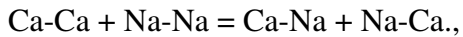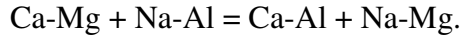
To determine the set of the Js and A_{ij} we have calculated for each of the 800 structures the fractions (frequencies of occurrence) of pairs of dissimilar atoms for the 37 structurally different pairs. In the case of the inter-site interaction we calculated the sum of the frequencies of Ca-Al and Na-Mg pairs. The distances and the types of interactions of the pairs are specified in Table 3. The whole set of configurations was thus characterized by the 800×38 frequency-composition matrix $\mathbf{P}$ and with the 800-element vector $\mathbf{E}$. With each dissimilar pair we associate a constant J_n and with the composition parameter x_i we associate E_0. The 37-element vector $\mathbf{J}$ was found by solving the matrix equation $\mathbf{J}=\mathbf{P}^{-1}\mathbf{E}$ using a least squares method. In these calculations we have at first fixed A_{12} and A_{21} (and the E_0 term) at some arbitrary values and subtracted E_0 from each E_i value. The least squares procedure was then repeated for different values of A_{12} and A_{21}. Their optimal values were found using a steepest dissent algorithm.

The ground state analysis

In order to improve the accuracy of the cluster expansion and to ensure that it predicts correct ground states, we have used a feed-back algorithm, which was described in detail by Vinograd et al. (2006). This algorithm consists of alternating Monte Carlo annealing simulations (see the next paragraph) and GULP energy minimization calculations. The cation distribution is annealed within the small 2x2x4 supercell at a low temperature consistently with the current values of $J_{(n)}$ constants and A_{12} and A_{21} parameters. The simulated low-temperature configuration is used as an input for a new GULP calculation. The energy of this structure and the frequency numbers are added to the set of previously simulated structures. A new least-squares solution is obtained and the Monte Carlo annealing is repeated with the new values of J_n, A_{12} and A_{21} parameters. The

algorithm allows an effective search for the lowest energy structure consistent with the chosen type of the cluster expansion. The energies of the found low energy states are interpolated with the solid lines (Fig. 1). The ground states are indicated with the dashed line. The $J_{(n)}$, values calculated with this algorithm are listed in Table 5 and plotted in Fig. 2. These values are consistent with $A_{12} = 2.6715$ and $A_{21} = 2.2193$ kJ/mol. The accuracy of the fit is illustrated in Fig. 3. We assume that the energy of any other possible configuration not included in the fit will be also accurately approximated with Equation 2. This allows us to efficiently simulate the Boltzmann probability distribution of the exchangeable atoms with the Monte Carlo algorithm.

The enthalpy of mixing

Monte Carlo simulations have been performed using $8 \times 8 \times 12$ supercell with periodic boundary conditions (6144 exchangeable sites). The swapping of sites has been performed according to the Metropolis algorithm (Metropolis et al. 1953). The energy differences between the subsequent steps have been calculated using Equation 2. The temperature dependent properties have been calculated on a grid of 65 different compositions across the diopside-jadeite binary in the interval of 273–2023 K with a step of 50 K. Each point in T-X space was equilibrated for $4*10^7$ Monte Carlo steps and additional $4*10^7$ steps were used for the calculation of the averages. The averaging over the Monte Carlo results gives the isotherms of the excess static lattice energy. These isotherms are compared with the experimentally measured enthalpies in Figure 4. The rapid decrease in the excess energy at the intermediate composition is interpreted as the effect of LRO.

Long-range order

The LRO variation across the transition was investigated only at the 50/50 composition (Fig. 5).

The order parameters have been defined using the Equation 1. The probabilities of Ca in the sub-sites M11 and M12 and Mg in M21 and M22 become structurally distinct only in the *P2/n* phase, thus both the LRO parameters are zero in the *C2/c* phase. The occupancies of the sub-sites and the LRO parameters have been calculated indirectly from the probabilities (frequencies) of AA pairs at the maximum separation (19.5565 Å) permitted by the size of the supercell using the equation

$$P_{AA} = P_A^{Mi1} P_A^{Mi2} = P_A^2 (1 + Q_i)(1 - Q_i) = (1 - Q_i)^2 / 4 \qquad (4)$$

where P_A is the probability of finding an A atom in the whole lattice ($P_A = 1/2$ at the intermediate composition). This method was preferred over the direct summation over the Monte Carlo simulated configurations to avoid the effect of spontaneous reversals in the orientation of LRO. When the reversal of ordering occurs, the site which was Na-rich becomes Ca-rich. Thus, the average (over the simulation time) site occupancies approach the average mole fractions over the lattice. Similar reversals are responsible for the development of anti-phase domains in natural samples (Carpenter, Muller). The rapid drop of the both LRO parameters at about 1150+20 K corresponds to the SRO/LRO transition. The nonzero values of the LRO parameter at the higher temperatures are due to the finite size of the simulation cell.

The free energy of mixing and the configurational entropy

It has been shown (Myers et al., 1998; Warren et al., 2001) that the configurational free energy can be calculated from Monte Carlo averaged excess energies using the method of thermodynamic integration:

$$G = G_0 + \int_0^\lambda \langle H \rangle_\lambda d\lambda \qquad (5)$$

In this equation, G_0 corresponds to the free energy of mixing of the solid solution with zero ordering energy, which can be calculated theoretically:

$$G_0 = RT(x_{Ca} \ln x_{Ca} + x_{Na} \ln x_{Na}) \tag{6}$$

To calculate $\langle H \rangle_\lambda$ for a state with an intermediate degree of order defined by certain value of λ, $0 < \lambda < 1$, one performs additional Monte Carlo simulations with scaled values of the Js:

$$J_n^\lambda = \lambda J_n \tag{7}$$

In our simulations, λ was gradually increased from 0 to 1 with a step of 0.04. The integral was calculated using Simpson's method. Figure 6 shows the free energy of mixing. These free energies include the effect of the configurational entropy which can be calculated with the equation.

$$S = (G - \langle H \rangle)/T \tag{8}$$

This function is plotted in Fig. 7. The configurational entropy reflects the effects of SRO and LRO. The development of LRO is manifested by the rapid decrease in the entropy at the intermediate composition.

The phase diagram

The free energies of mixing were converted to a *T-X* phase diagram by comparing the free energy, $G(x_i)$, at each composition x_i along an isotherm is to the free energy of a mechanical mixture $G(x_j) + G(x_k)$. If there is a pair of compositions x_j and x_k, which satisfy the conditions $x_j < x_i < x_k$ and $[G(x_j)(x_k - x_i) + G(x_k)(x_i - x_j)] < F(x_i)$, the solution with composition x_i is unstable. The miscibility gaps are shown as smoothed curves, which encircle the clusters of the unstable points (Fig. 8).

The activity-composition relations

The calculation of activities requires the isotherms of the free energy to be expressed as analytical functions of composition. The excess free energies calculated by subtracting the $-TS_{ideal}$ term from the Monte Carlo free energies are plotted in Figure 9. At temperatures above 800 °C, the excess free energies behave smoothly. These functions can be made perfectly symmetric with respect to $x_1=0.5$ by subtracting the E_0 term. Therefore, an accurate fit to $G_{excess} - E_0$ can be achieved with the polynomial, which contains only even powers of $(x_2 - x_1)$:

$$G_{excess} = x_1 x_2 \sum_{n=1}^{3} (A_n + TB_n)(x_2 - x_1)^{2n-2} + E_0 \tag{9}$$

where x_1 and x_2 are mole fractions of diopside and jadeite, respectively. The coefficients of this polynomial are given in Table 5. At lower temperatures the excess functions become affected by omphacite-type ordering. In the temperature range of 300 - 800 °C a good fit can be achieved with a more complex function:

$$G_{excess} = x_1 x_2 \sum_{n=1}^{3} (A_n + TB_n)(x_2 - x_1)^{2n-2} + x_1 x_2 \sum_{m=1}^{2} (C_m + TD_m) \exp\left[(E_m + TF_m)(x_2 - x_1)^{2m}\right] + E_0 \tag{10}$$

The coefficients of this polynomial are given in Table 5. In Figures 10 and 11 the activities at 600 and 1200 °C, calculated using the Eqns. 10 and 9, respectively, are plotted as dashed lines together with the experimental data of Holland (1983) and Gasparik (1985). Note, that in Fig. 10 we plot the square root of activity. This is done to make the comparison with the original data of Holland (1983) easier. Apparently, the experimental data suggest a much stronger deviation from the ideal mixing than the calculated activities imply. This result suggests that the model misses a negative contribution to the excess free energy.

The excess vibrational enropy

The missing negative contribution to the excess free energy could come from the excess

vibrational entropy, the effect, which has not been included in our model yet. The recent

simulation study of mixing in pyrope-grossular garnets (Vinograd and Sluiter, 2006) suggested

that measurable positive excess vibrational entropy is to be expected in solid solutions with large

volume mismatch between the end-members. This should be also the case for the diopside-jadeite

solid solution. The model of Vinograd and Sluiter (2006) suggests that the excess effect appears

due to the deformation of the lattices of end-members in the process of mixing when they

accommodate to certain intermediate volume within the solid solution. The lattice of the end-

member with the smaller volume (jadeite) extends, while the lattice of the end-member with the

larger volume (diopside) contracts. The increase in the vibrational entropy of the smaller end-

member on the extension outweighs the corresponding decrease in the entropy of the larger end-

member on the contraction. Consequently, the total effect, calculated as the weighted average of

the excess vibrational entropies of the end-members, is positive. Fig. 12 illustrates this effect for

the strained mixture of diopside and jadeite at 1073 K. The total effect is positive with the

maximum shifted prominently in the direction of the larger end-member. The excess entropy

achieves about 0.9 J/K per one mole of exchangeable cations at 40 mole % of the jadeite

component. Similar calculations performed between 873 and 1473 K suggested that the

magnitude of the excess effect remains essentially the same within this temperature range. The

shape of the function can be closely described with a superquadratic Margules equation

$$S_{excess}^{vib} = x_1 x_2 (x_1 S_{12} + x_2 S_{21})$$ (11)

with the parameters $S_{12} = 2.5$ and $S_{21} = 4.5$ J/mol/K. The activity-composition functions modeled

with the excess entropy effect, $-TS_{excess}^{vib}$, (solid lines in Figures 10 and 11) agree much better with

the experimental activities both at 873 and 1283 K. The activity-composition relations in the

range of 300-800 °C are plotted in Fig. 13.

Discussion and Conclusions

The present model reproduces several experimental constraints with a remarkable accuracy. The predicted magnitude of the high-temperature enthalpy of mixing in the diopside – jadeite system is consistent with the calorimetric data of Wood et al. (1980). The calculated activity-composition relations at 600 and 1200 °C can be brought into an agreement with the experimental data of Holland (1983) and Gasparik (1985) by assuming the existence of a reasonably large excess vibrational entropy term. The magnitude of this term (0.9 J/mol/K) agrees well with the calculated effect for the strained mixture of diopside and jadeite. The excess entropy of similar magnitude has been experimentally measured in pyrope – grossular system (Haselton and Westrum, 1980; Dachs and Geiger, 2006). The difference in the standard volumes between diopside and jadeite is comparable to that between pyrope and grossular, and, therefore, this effect is not unexpected. We observe that the activities, modified by including the excess vibrational entropy, agree better with the experiments of Gasparik (1985) at 1200 °C than with the experiments of Holland (1983) at 600 °C. We should note that the present treatment of the excess entropy does not include effects of structural relaxation. These effects are likely to decrease the excess entropy at intermediate compositions and low temperatures as it was predicted for pyrope-grossular garnets (Vinograd and Sluiter, 2006). The effect of relaxation has not been included here because its evaluation would require free energy minimization of a large number of possible configurations within the supercell containing 640 atoms. These calculations would require too much time. We think that such an effort will be justified when the effect of the excess vibrational entropy is detected experimentally.

The onset of LRO at the omphacite composition is predicted at 1150 +20 K in close

agreement with the experimental value (1123 +20 K) of Carpenter (1981). Moreover, the

simulations confirm the experimental finding of Rossi et al. (1983), Carpenter et al. (1990) and

Boffa Ballaran et al. (1998) that the M2 site is ordered significantly stronger than the M1 site.

The approximate relationship $Q_{M2}=2Q_{M1}$ in closely reproduced in our simulations (Fig. 14). The

simulations not only reproduce the experimental facts, but also suggest their atomistic

interpretation. Apparently, the stronger ordering within the M2 site is consistent with to the first-

neighbour M2-M2 distance being significantly shorter than the M1-M1 distance. Figure 2 shows

that the strength of ordering interactions increases at shorter distances. This is consistent with the

earlier result of Cohen and Burnham (1986) who obtained -36 kJ/mol and -10 kJ/mol for the

nearest-neighbour M2-M2 and M1-M1 interactions, respectively, using an approach similar to

that used here. Therefore, the $Q_{M2}=2Q_{M1}$ relationship can be understood on energy grounds and

there is no need in postulating the existence of a rigid crystal-chemical rule, which restricts the

M1 site to be half-ordered. The simulations suggest, however, that the true ground state with

$Q_{M2}=Q_{M1}=1$ is never achieved in nature. The slowing down of the kinetics of ordering with the

decrease in the temperature seems to be the most likely explanation. The simulations permit to

map the spread of the experimental ordering states onto the temperature scale (Fig. 14). The plot

suggests that the closing temperature of the cation ordering in omphacite is about 600 °C.

Many previous studies have noted the coexistence of the ordering and exsolution tendencies

in the system. The model of Vinograd (2002) attributed the exsolution tendency to the non-

configurational effect related to volume difference between diopside and jadeite. It has been

argued that the size-mismatch implies investment of a significant energy needed to overcome the

misfit between the lattices. (The magnitude of this effect is comparable to the excess enthalpy

measured by Wood et al., 1980). Our model contains the special term, E_0, which is supposed to

model this non-configurational effect. Surprisingly, the best-fit A_{ij} values, which are responsible

for the magnitude and asymmetry of this term, appeared to be very small. This result suggests

that the volume deformation energy is absorbed by the values of Js. The elastic effect has

probably contributed to the cross-site (M1-M2) terms which correspond to the long-distance

pairs. The long distance pairs are nearly insensitive to order and contribute to the enthalpy of

mixing as $x_1 x_2 J^*$, where J^* is an effective long-distance interaction. Since the asymmetry of the

data is very small, the elastic term, which has the same shape, can be easily shadowed with the

$x_1 x_2 J^*$ term. The present results suggest also that the positive high-temperature enthalpy of

mixing appears not only due to the size-mismatch, but also due to the charge mismatch effect.

The positive cross-site Js evidently have a strong electrostatic component. It is easy to see that

the charge difference contributes to the enthalpy effect of the reciprocal reaction, $Ca^{2+}Mg^{2+} +$

$Na^+Al^{3+} = Ca^{2+}Al^{3+} + Na^+Mg^{2+}$. For a given interatomic distance the total electrostatic energy of

the pairs Ca-Al and Na-Mg is higher than the sum of the energies of Ca-Mg and Na-Al pairs.

(After subtracting the average charge of 2+ from the formal cation charges, the reciprocal

reaction can be written as $Ca^{0+}Mg^{0+} + Na^{1-}Al^{1+} = Ca^{0+}Al^{1+} + Na^{1-}Mg^{0+}$. The electrostatic energy

of Na-Al pair is negative, while the energies of all the other pairs are zero. Thus the total

electrostatic effect of the reaction is positive.) This implies that the formation of a two-site solid

solution with mixed-valent substitution proceeds against the electrostatic force and, therefore, the

charge difference additionally contributes to the strain produced by the size mismatch. At

intermediate compositions this effect appears to be counterbalanced with the effect of ordering.

The ordering is apparently driven by the electrostatic advantage of charge alternation along the

chains of M1 and M2 sites. Two mixed-charged Ca^{2+}-Na^+ pairs have lower Coulomb energy than

the sum of energies of Na^+-Na^+ and Ca^{2+}-Ca^{2+} pairs. Likewise, two Mg^{2+}-Al^{3+} pairs have lower

energy than the sum of energies of Mg^{2+}-Mg^{2+} and Al^{3+}-Al^{3+} pairs. (This can be clearly seen

when the average charge of +2 is subtracted from the formal cation charges.) This observation

explains the negative sign of the Js related to the reactions NaNa + CaCa = 2NaCa and MgMg + AlAl = 2 MgAl. Thus, both the positive enthalpy of mixing (the tendency to exsolution) and the long-range ordering appear to be the consequences of the charge difference between the cations occupying M1 and M2 sites. Since the charge difference itself is the consequence of the coupled substitution, the positive enthalpy at high temperatures and the ordering at low temperatures and intermediate compositions should be expected in any two-site solid solution build along the same mechanism.

The present study shows that the approach based of the application of the static lattice energy minimization, cluster expansion and Monte Carlo simulations reproduces known experimental data on the effects of ordering and mixing in the diopside-jadeite system with good accuracy. This implies that the same approach can be applied to other binary clinopyroxene solid solutions for which these effects are not yet known.

References

Angel, R.J., Carpenter, M.A., and Finger, L.W. (1990) Structural variation associated with compositional variation and order-disorder behavior in anorthite-rich feldspars American Mineralogist, 75, 150–162.

Bass, J.D. (1995) Elasticity of minerals, glasses, and melts. In Th. Ahrens, Ed., Mineral Physics and Crystallography. A Handbook of Physical Constants. AGU Reference Shelf 2. 45 p. American Geophysical Union, Washington, D.C.

Becker, U., Fernandez-Gonzalez, A., Prieto, M., Harrison, R., and Putnis, A. (2000) Direct calculation of thermodynamic mixing properties of the barite/celestite solid solution from molecular principles. Physics and Chemistry of Minerals, 27, 291-300.

Boffa Ballaran, T., Carpenter, M.A., Domeneghetti, M.C., Tazzoli, V. (1998) Structural mechanisms of solid solution and cation ordering in augite-jadeite pyroxenes: I. A macroscopic perspective. *American Mineralogist*, **83**, 419–433.

Bosenick, A., Dove, M.T., Myers, E.R., Palin, E.J., Sainz-Diaz, C.I., Guiton, B.S., Warren, M.C., and Craig, M.S. (2001a) Computational methods for the study of energies of cation distributions: applications to cation-ordering phase transitions and solid solutions. Mineralogical Magazine, 65, 193–219.

Bosenick, A., Dove, M.T., Heine, V., and Geiger, C.A. (2001b) Scaling of the thermodynamic mixing properties in garnet solid solutions. Physics and Chemistry of Minerals, 28, 177–187.

Cameron M., Sueno, S., Prewitt, C. T., Papike, J.J. (1973) High-temperature crystal chemistry of acmite, diopside, hedenbergite, jadeite, spodumene, and ureyite. American Mineralogist, 58, 594-618.

Carpenter, M.A. (1981) Time-Temperature-Transformation (TTT) analysis of cation disordering in omphacite. Contributions to Mineralogy and Petrology, **78**, 433-440.

Carpenter, M.A., Dmeneghetti, M.C., Tazzolli, V. (1990) Application of Landau theory to cation ordering in omphacite I: Equilibrium behaviour. European Journal of Mineralogy, **2**, 7-18.

Cohen, R.E., Burnham C.W. (1985) Energetics of ordering in aluminous pyroxenes. American Mineralogist, **70** 559-567.

Connolly J.W.D., Williams, A.R. (1983) Density-functional theory applied to phase transformations in transition-metall alloys. Phys. Rev. B27 5169-5172.

Dachs, E., and Geiger, C.A. (2006) Heat capacities and entropies of mixing of pyrope-grossular ($Mg_3Al_2Si_3O_{12}$-$Ca_3Al_2Si_3O_{12}$) garnet solid solutions: A low-temperature calorimetric and a thermodynamic investigation. American Mineralogist, 91, 894–906.

Dove M.T. (2001) Computer simulations of solid solutions. In Ch. Geiger, Ed., Solid Solutions in Silicate and Oxide Systems of Geological Importance. EMU Notes in Mineralogy, 3, 225 p. Eötvös University Press, Budapest.

Ferreira, L.G., Mbaye, A.A., and Zunger, A. (1988) Chemical and elastic effects on isostructural phase diagrams: The e-G approach. Physical Review B, 37, 10547–10570.

Gale, J.D. (1996) Empirical derivation of interatomic potentials for ionic materials. Philosophical Magazine B, 73, 3–19.

Gale, J.D. (1997) GULP—a computer program for the symmetry adapted simulation of solids. Journal of Chemical Society: Faraday Transactions, 93, 629–637.

Ganguly, J. (1973) Activity-composition relation of jadeite in omphacite pyroxene: Theoretical deductions. Earth and

    Planet. Sci. Lett. **19** 145-153.

Gasparik, T. (1985) Experimentally determined compositions of diopside-jadeite pyroxene in equilibrium with albite

    and quartz at 1200-1350°C and 15-34 kbar. Geochim. Cosmochim. Acta **49** 865-870.

Harlow G E, Brown G E (1980) Low albite: An X-Ray and neutron diffraction study. American Mineralogist, 65, 986-

    995.

Haselton, H.T. Jr. and Westrum, E.F. Jr. (1980) Low-temperature heat capacities of synthetic pyrope, grossular, and

    $pyrope_{60}grossular_{40}$. Geochimica et Cosmochimica Acta, 44, 701–709.

Holland, T.J.B. (1983) The experimental determination of activities in disordered and short-range ordered jadeitic

    pyroxenes. Contrib. Miner. Petrol. **82** 214-220.

Lavrentiev, M.Yu., van Westrenen, W., Allan, N.L., Freeman, C.L., and Purton, J.A. (2005) Simulation of

    thermodynamic mixing properties of garnet solid solutions at high temperatures and pressures. Chemical Geology,

    225, 336-346.

Levien L., Weidner, D.J., Prewitt, C.T. (1979) Elasticity of diopside. Physics and Chemistry of Minerals, 4, 105-113.

Kandelin, J., Weidner,D.J. (1988) The single-crystal elastic properties of jadeite. Phys. Earth Planet Int. 50, 251-260.

Kushiro, I. (1969) Clinopyroxene solid solutions formed by reactions between diopside and plagioclase at high

    pressures. Mineralogical Society of America Special Paper, **2**, 179-191.

Metropolis, N.I., Rosenbluth, A.W., Rosenbluth, M.N., Teller, A.N. and Teller, E. (1953) Equation of state calculations

    by fast computing machines. Journal of Chemical Physics 21, 1087–1092.

Myers, E.R., Heine, V., and Dove, M.T. (1998) Some consequences of Al/Al avoidance in the ordering of Al/Si

    tetrahedral framework structures. Physics and Chemistry of Minerals, 25, 457–464.

Patel, A., Price, G.D., and Mendelsson. M.J. (1991) A computer-simulation approach to modeling the structure,

    thermodynamics and oxygen isotope equilibria of silicates. Physics and Chemistry of Minerals, 17, 690–699.

Rodehorst, U., Geiger, C.A., and Armbruster, T. (2002) The crystal structures of grossular and spessartine between 100

    and 600 K and the crystal chemistry of grossular-spessartine solid solutions. American Mineralogist, 87, 542–549.

Rossi, G., Smith, D.C., Ungaretti, L., Domeneghetti, M.C. (1983) Crystal-chemistry and cation ordering in the system

    diopside-jadeite: A detailed study by crystal structure refinement. Contributions to Mineralogy and Petrology, **83**,

    247-258.

Swainson, I.P., Dove, M.T., Schmahl, W.W., Putnis, A. (1992) Neutron diffraction study of the akermanite-gehlenite

solid solution series. Physics and Chemistry of Minerals, 19, 185–195.

Sanders, M.J., Leslie, M., and Catlow, C.R. (1984) Interatomic potentials for SiO_2. Journal of the Chemical Society, Chemical Communications, 19, 1271–1273.

Sainz-Diaz, C.I., Hernandez-Laguna, A., and Dove, M.T. (2001) Modeling of dioctahedral 2:1 phyllosilicates by means of transferable empirical potentials. Physics and Chemistry of Minerals, 28, 130–141.

Sanchez J.M., Ducastelle, F., Gratias, D. (1984) Generalized cluster description of multicomponent systems Physica 128A, 334-350

Vinograd, V.L., Sluiter, M.H.F. (2006) Thermodynamics of mixing in pyrope-grossular, $Mg_3Al_2Si_3O_{12}$- $Ca_3Al_2Si_3O_{12}$, solid solution from lattice dynamics calculations and Monte Carlo simulations. Amer. Mineral. **91** 1815-1830.

Vinograd, V.L., Sluiter, M.H.F., Winkler, B., Putnis, A., and Gale, J.D. (2004) Thermodynamics of mixing and ordering in silicates and oxides from static lattice energy and ab initio calculations. In M. Warren, A. Oganov and B. Winkler, Eds., First-Principles Simulations: Perspectives and Challenges in Mineral Sciences. Deutsche Gesellschaft für Kristallographie. Berichte aus Arbeitskreisen der DFK, 14, 143 p.

Vinograd, V.L.,Winkler, B., Putnis, A., Kroll, H., Milman, V., Gale, J.D., and Fabrichnaya, O. B. (2006) Thermodynamics of pyrope-majorite, $Mg_3Al_2Si_3O_{12}$-$Mg_4Si_4O_{12}$, solid solution from atomistic model calculations. Molecular Simulations, 32 (2) 85-99.

Vinograd, V.L., Burton, B.P., Gale, J.D., N.L. Allan, Winkler, B. (2007) Activity-composition relations in the system CaCO3- predicted from static structure energy calculations and Monte Carlo simulations. Geochimica et Cosmochimica Acta (in press).

Vinograd, V.L., Winkler, B., Putnis, A., Gerya, T., Perchuk, L.L. (2007) Order/disorder transition in cordierite and its possible relationship with the development of symplectites of cordierite and orthopyroxene in granulites. Petrology. (2007) (submitted).

Warren, M.C., Dove, M.T., Myers, E.R., Bosenick, A., Palin, E.J., Sainz-Diaz, C.I., and Guiton, B.S. (2001) Monte Carlo methods for the study of cation ordering in minerals. Mineralogical Magazine, 65, 221–248.

Winkler, B., Dove, M.T., and Leslie, M. (1991) Static lattice energy minimization and lattice dynamics calculations on aluminosilicate minerals. American Mineralogist, 76, 313–331.

Wood, B.J., Holland, T.J.B., Newton, R.C., Kleppa, O.J. (1980) Thermochemistry of jadeite-diopside pyroxenes. Geochimica et Cosmochimica Acta, **44**, 1363-1371.

Figure captions

Figure 1. The excess energies of the sampled structures (*circles*). Solid line connects the low-energy structures predicted using the Monte Carlo annealing algorithm. The dashed line connects the ground states. All values are per mole of M1 cations.

Figure 2. The cluster expansion of the pair-wise effective interactions for the diopside-jadeite system as functions of the interatomic separation. The distances have been calculated for the diopside composition ($a = 9.750$ Å, $b = 8.928$ Å, $c = 5.277$ Å, $\beta = 106.13°$).

Figure 3. Correlation between the energies calculated within the static energy calculation approach and those predicted with the cluster expansion.

Figure 4. Isotherms of the enthalpy of mixing (solid lines) predicted with Monte Carlo simulations. Squares with error bars are the calorimetric measurements of Wood et al. (1980).

Figure 5.. The temperature dependence of the LRO parameters Q_{M1} (open circles) and Q_{M2} (filled circles) as calculated for omphacite composition from Monte Carlo simulations.

Figure 6. Gibbs free energy of mixing derived from the thermodynamic integration analysis of the Monte Carlo results.

Figure 7. The configurational entropy calculated using the method of thermodynamic integration.The dashed line shows the entropy of ideal mixing.

Figure 8. The temperature-composition phase diagram calculated from the results of Monte Carlo simulations (solid lines). The dotted lines show the shift of the miscibility gaps due to the effect of the excess vibrational entropy. The dashed line shows the approximate location of the order/disorder transition.

Figure 9. The excess free energy of mixing as calculated from the Monte Carlo simulations. The effect of the excess vibrational entropy is non included.

Figure 10. The square root activity of jadeite and diopside at 600 °C. The solid lines and dashed lines correspond to the calculation with and without the vibrational entropy term, respectively. The symbols correspond to the experimental phase equilibrium measurements of Holland (1983). The filled and open squares correspond to pyroxene compositions partially equilibrated from $NaAlSi_2O_6$-oversaturated and undersaturated starting materials, respectively.

Figure 11. The activities of jadeite and diopside at 1200 °C. The solid lines and dashed lines correspond to the

calculation with and without the vibrational entropy term, respectively. The circles correspond to the activities calculated using the equation of Gasparik (1985), that was used to fit his experimental data.

Figure 12. The entropic equations of state (entropy vs. volume) of diopside and jadeite and the total excess entropy plotted vs. the mole fraction of jadeite. The vibrational entropy is calculated at 1073 K. It is assumed that volume changes linearly with composition.

Figure 13. The activity-composition relations in the diopside-jadeite solid solution in the range of 300-800 °C calculated using Eqns. 10 and 11.

Figure 14. Correlation between the order parameters Q_{M1} and Q_{M2} as calculated from Monte Carlo simulations results and compared to the experimental data (crosses) of Boffa Ballaran et al. 1998.

Table 1. The empirical interatomic potentials used in the present study. The notation [4], [6] and [8] refers to the

coordination number of the associated species

Buckingham

Interaction	A (eV)	ρ (Å)	C (eV Å^6)
Al[4-6](core)-O(shell)	1115.6866	0.291905	0.0
Mg[6](core)-O(shell)	1190.5254	0.284037	0.0
Ca[6-8](core)-O(shell)	10050.3750	0.238457	0.0
Na[6-8](core)-O(shell)	9956.9835	0.218298	0.0
Si[4-6](core)-O(shell)	995.92238	0.304057	0.0
O(shell)-O(shell)	593.05553	0.321826	29.61488

Spring

Interaction	K (eV/Å^2)
O(core)-O(shell)	56.66397

Three-body

Interaction	k_θ (eV/rad^2)	θ (degree)
O(shell)-Si[4]-O(shell)	2.5171	109.47
O(shell)-Al[6]-O(shell)	1.4693	90.0
O(shell)-Mg[6]-O(shell)	1.0514	90.0

Note: The charges on the oxygen core and shell are 0.751575 and –2.451575, respectively. Cutoff distance for the Buckingham potentials is 12 Å.

Table 2. Structural parameters of diopside and jadeite as calculated with the SLEC in comparison with experimental

data.

Parameter	Diopside		Jadeite	
	XRD [a]	SLEC	XRD [a]	SLEC
a (Å)	9.745	9.750	9.423	9.386
b (Å)	8.899	8.928	8.564	8.532
c (Å)	5.251	5.277	5.223	5.266
β (degree)	105.63	106.13	107.56	107.76
Volume (Å^3)	438.532	441.303	401.848	401.615

References: [a]Cameron et al., 1973.

Table **3.** Elastic stiffness coefficients for diopside and jadeite as calculated with the SLEC in comparison with experimental data.

Stiffness coefficient	Observed[a]	SLEC	Observed[b]	SLEC
	Diopside		Jadeite	
C_{11}	223.0	202.2	274.0	238.2
C_{22}	171.0	182.4	253.0	261.2
C_{33}	235.0	285.9	282.0	313.4
C_{44}	74.0	75.9	88.0	92.1
C_{55}	67.0	56.7	65.0	66.5
C_{66}	66.0	61.5	94.0	69.9
C_{12}	77.0	65.0	94.0	72.9
C_{13}	81.0	61.3	71.0	82.7
C_{23}	57.0	68.3	82.0	110.4
C_{15}	17.0	29.22	4.0	31.1
C_{25}	7.0	15.9	14.0	22.1
C_{35}	43.0	27.5	28.0	-0.2
C_{46}	7.3	12.9	13.0	19.8
Bulk modulus	113.0	104.5	143.0	139.0

References: [a]Levien et al.1979; [b]Kandelin & Weidner 1988

Table **4.** The parameters of the fitted cluster expansion.

M1-M2		M1-M1		M2-M2	
d (Å)	J	d (Å)	J	d (Å)	J
3.191	17.116	4.555	−8.886	3.132	−19.864
4.455	14.324	4.908	−6.734	5.295	−5.433
4.494	7.266	5.295	−6.982	5.598	−4.508
5.488	5.482	5.868	−6.664	6.625	−7.122
5.544	6.756	6.237	−5.033	6.794	−3.159
6.177	5.072	6.625	−3.687	7.557	0.232
6.322	6.255	7.557	−3.042	7.737	0.198
6.749	2.083	8.083	−1.938	7.826	−0.561
7.626	1.449	8.764	−1.083	8.116	−2.406
7.634	2.330	8.943	−1.631	8.520	0.193
7.912	1.911			8.723	−0.190
8.140	1.906			8.943	−0.577
8.233	1.803				
8.485	1.304				
7.799	1.786				

Note: the J values are in kJ per mole of M1 cations.

Table 5. Coefficients of the polynomials for the excess free energy in the diopside-jadeite solid solution

N	A_n (J/mol)	B_n (J/mol·K)	A_n (J/mol)	B_n (J/mol·K)
	300-800°C		800-1400°C	
1	-3516.5	7.044	9878.1	5.19
2	18555.1	−8.831	11229	-3.092
3	7436.8	3.204	-496.2	2.359
4	-1654.3	1.433		
5	-130.7	0.0955		
6	3751.8	7.3267		
7	-4.4122	0.00313		

Note: The polynomials describe only the symmetric part of the excess free energy. To get full excess free energy, one has to add Margules equations for the elastic energy and the excess vibrational entropy.

Table 6. Coefficients of the Margules polynomials for the excess elastic energy and the excess vibrational entropy

ij	A_{ij} (kJ/mol)	S_{ij} (J/mol·K)
12	2.6715	2.5
21	2.2193	4.5
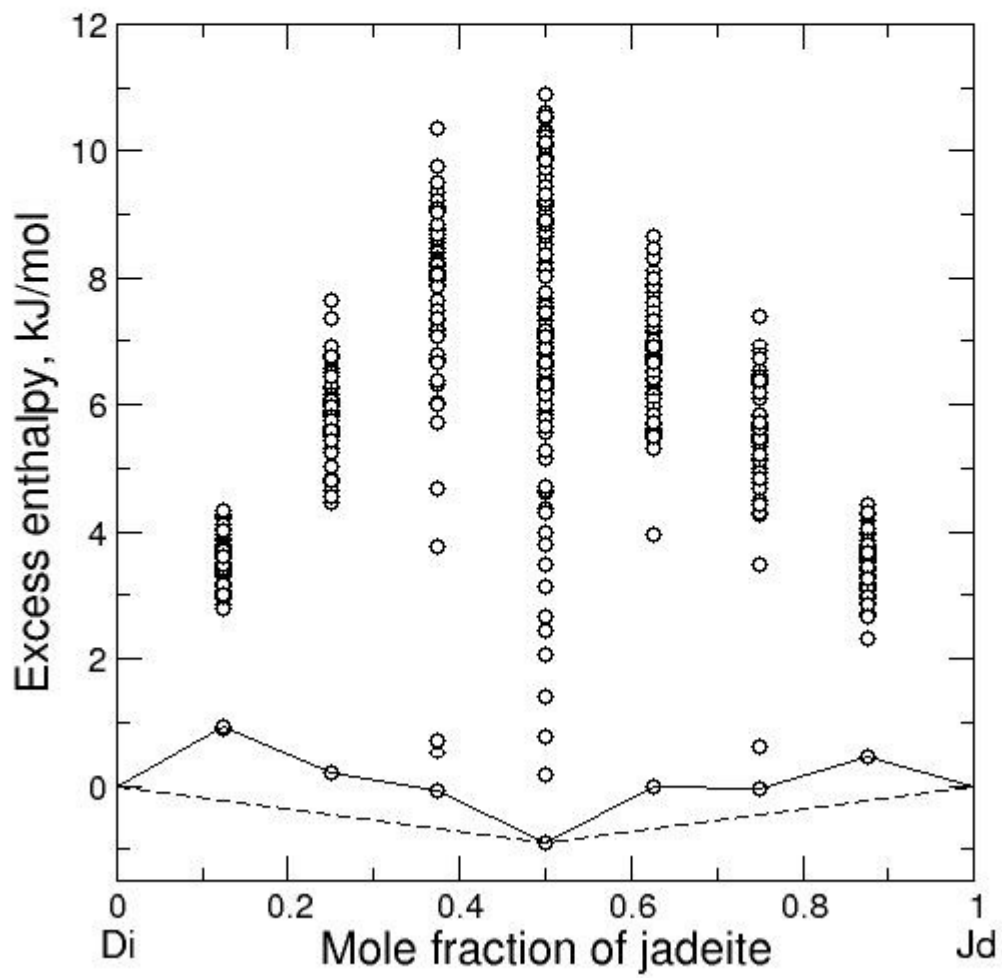
Figure 1
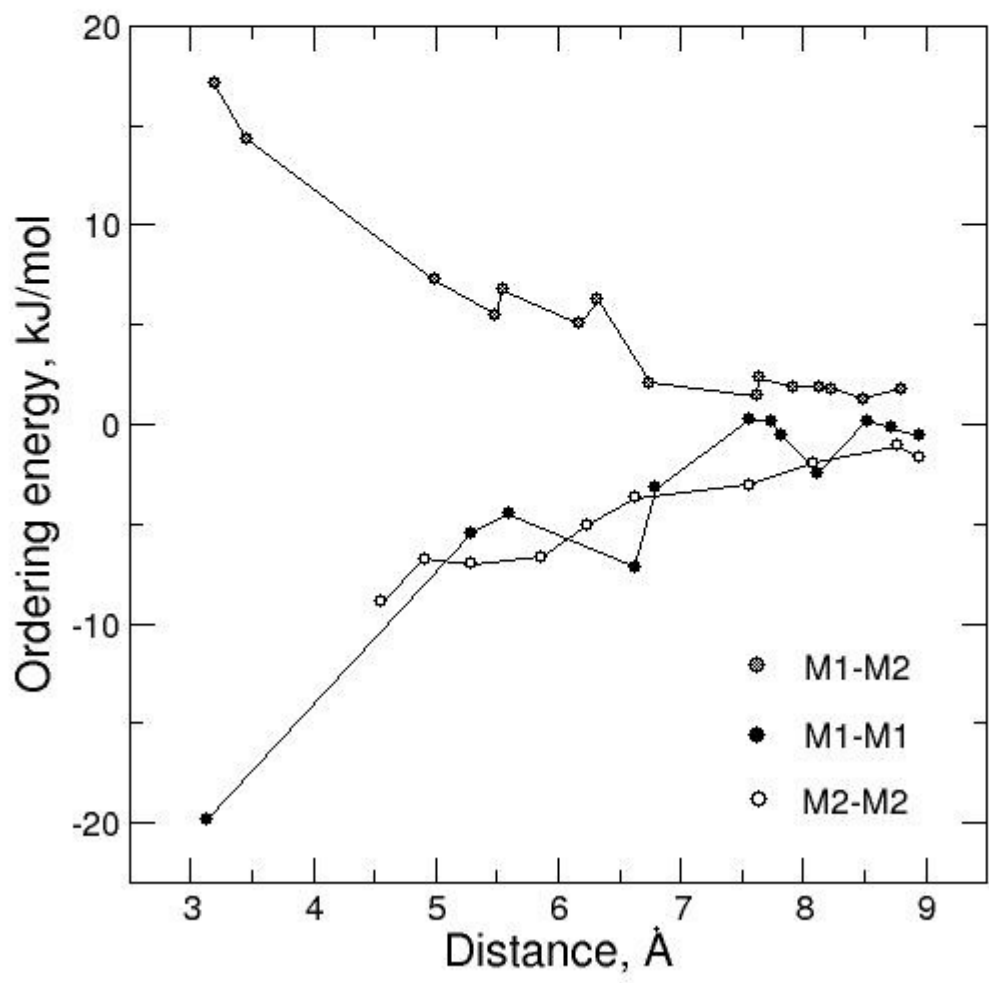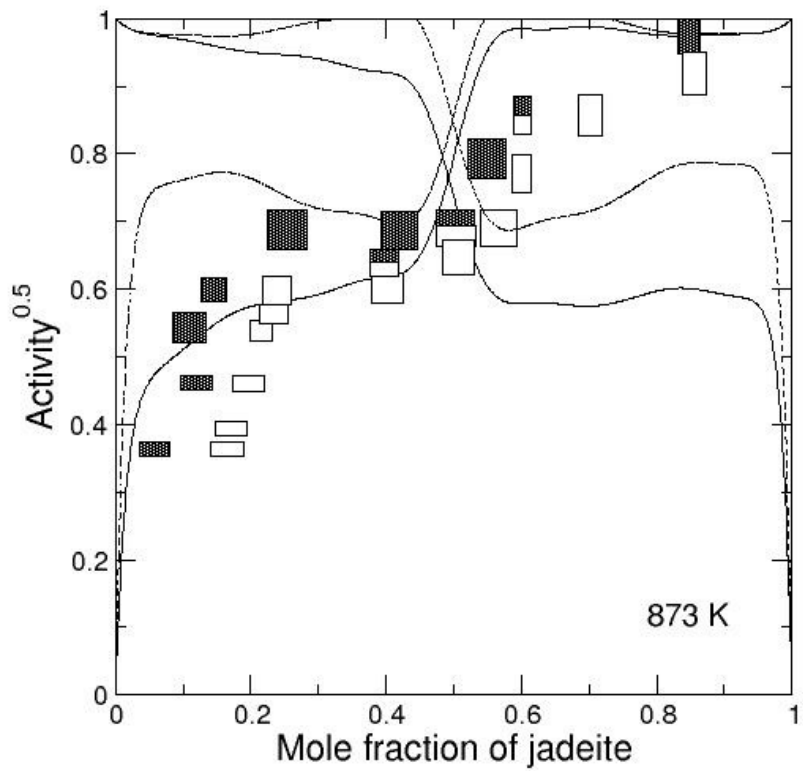
Figure 2
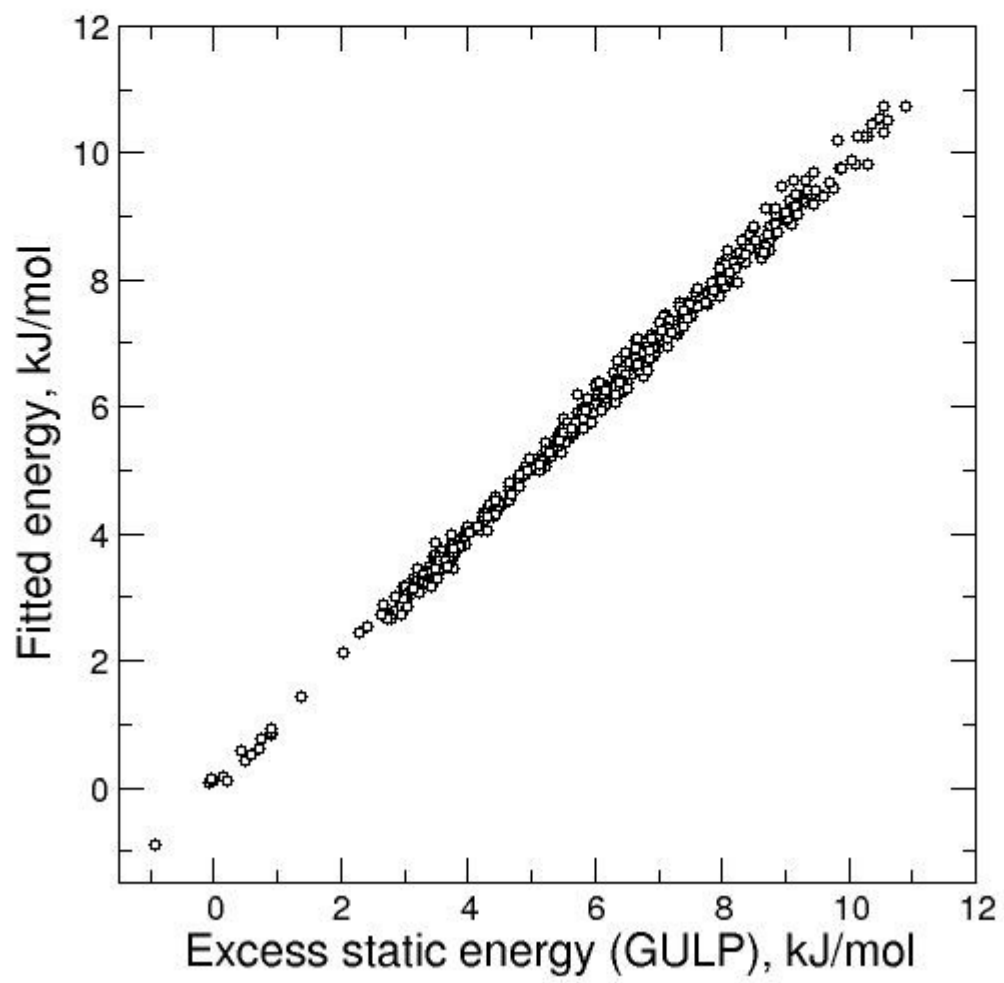
Figure 3
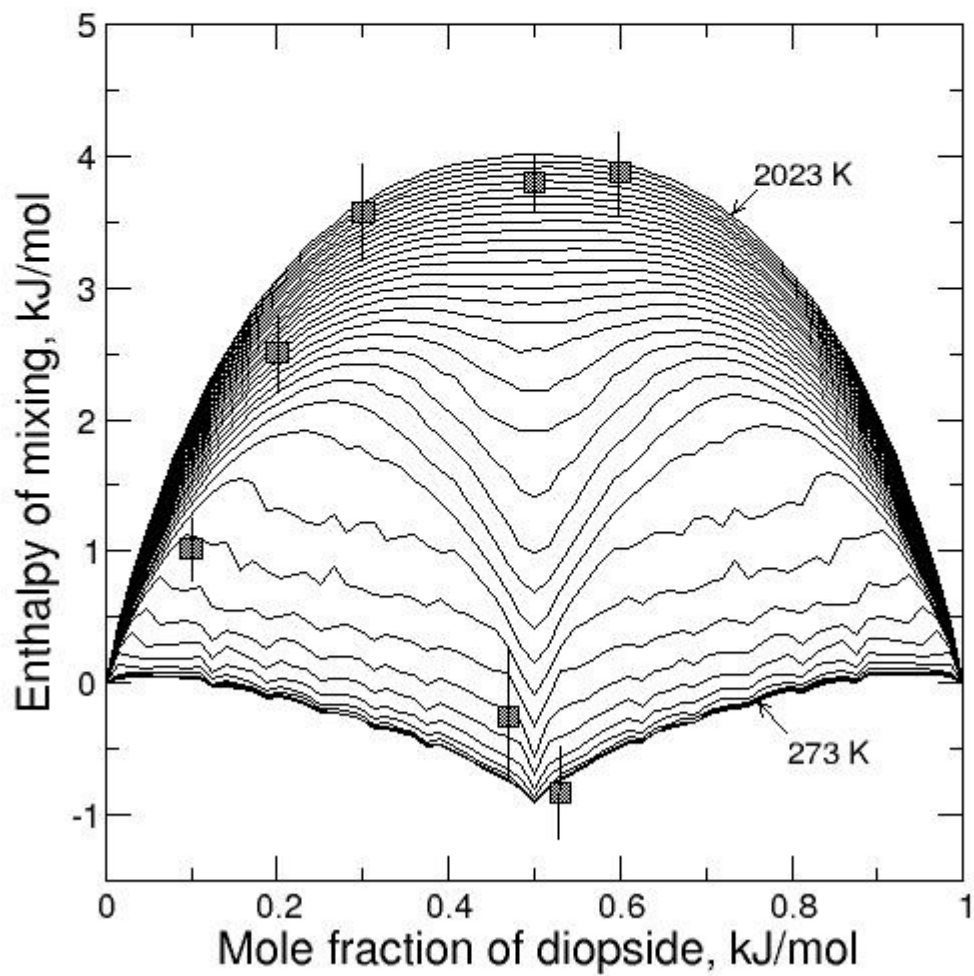
Figure 4.
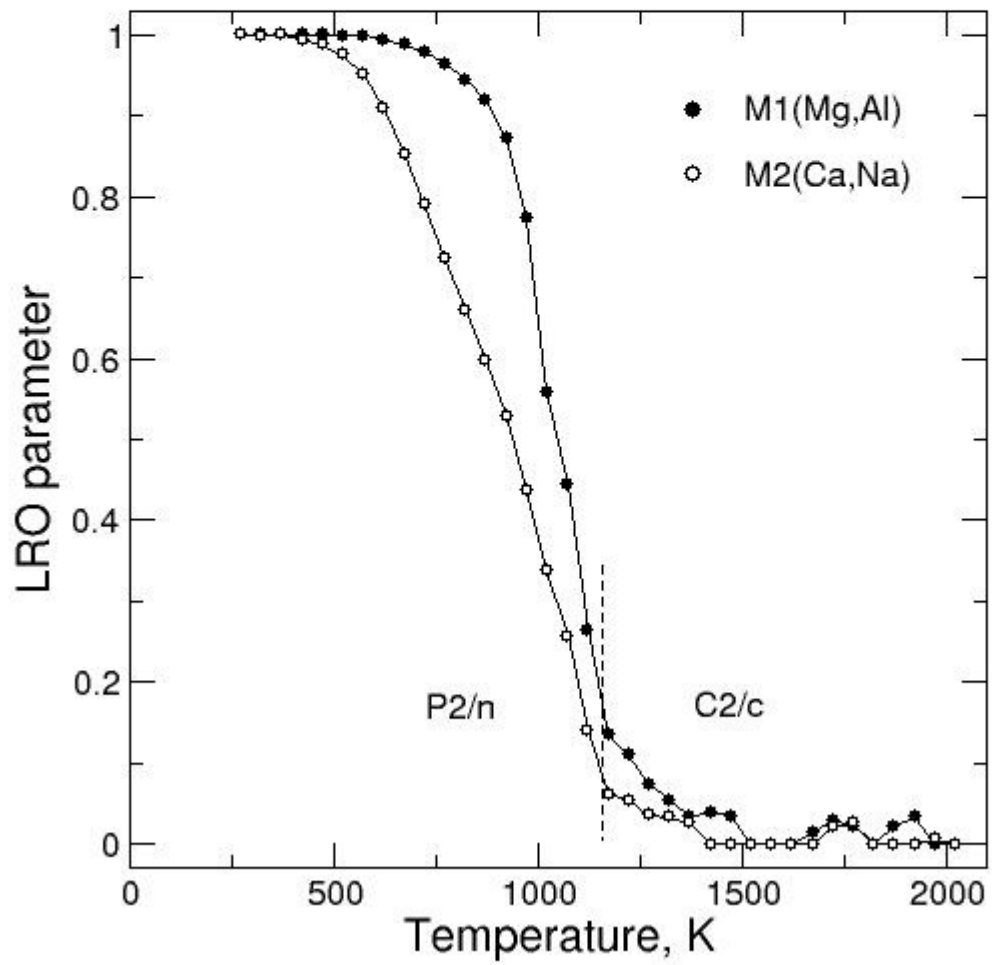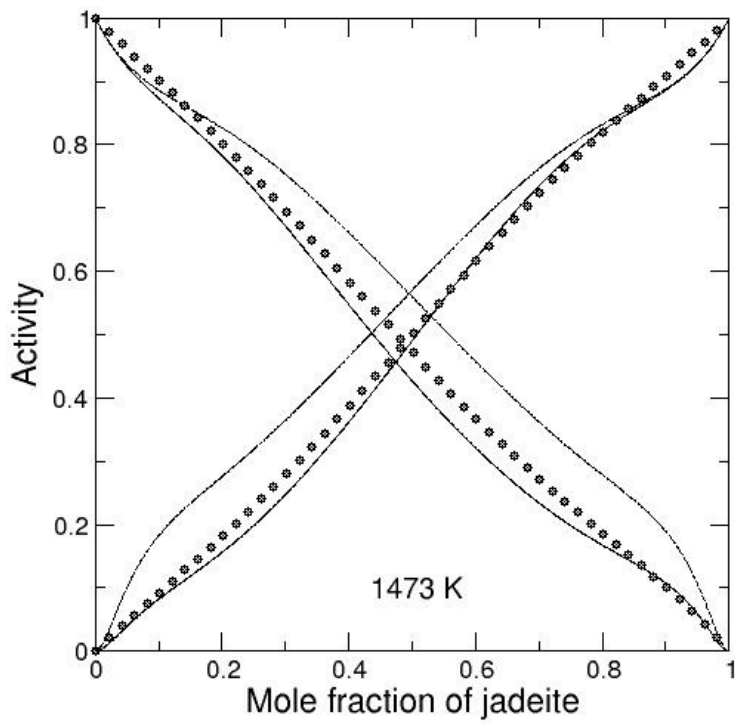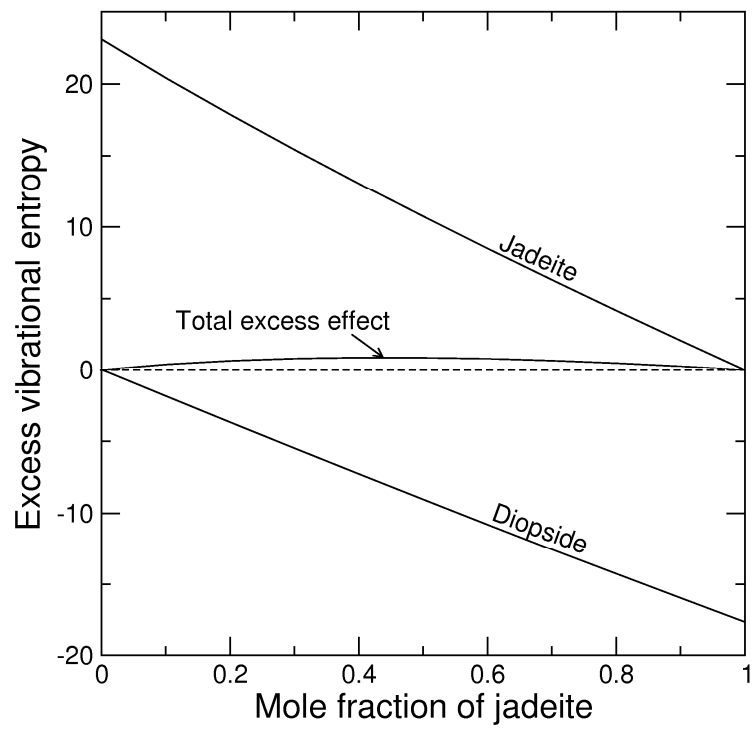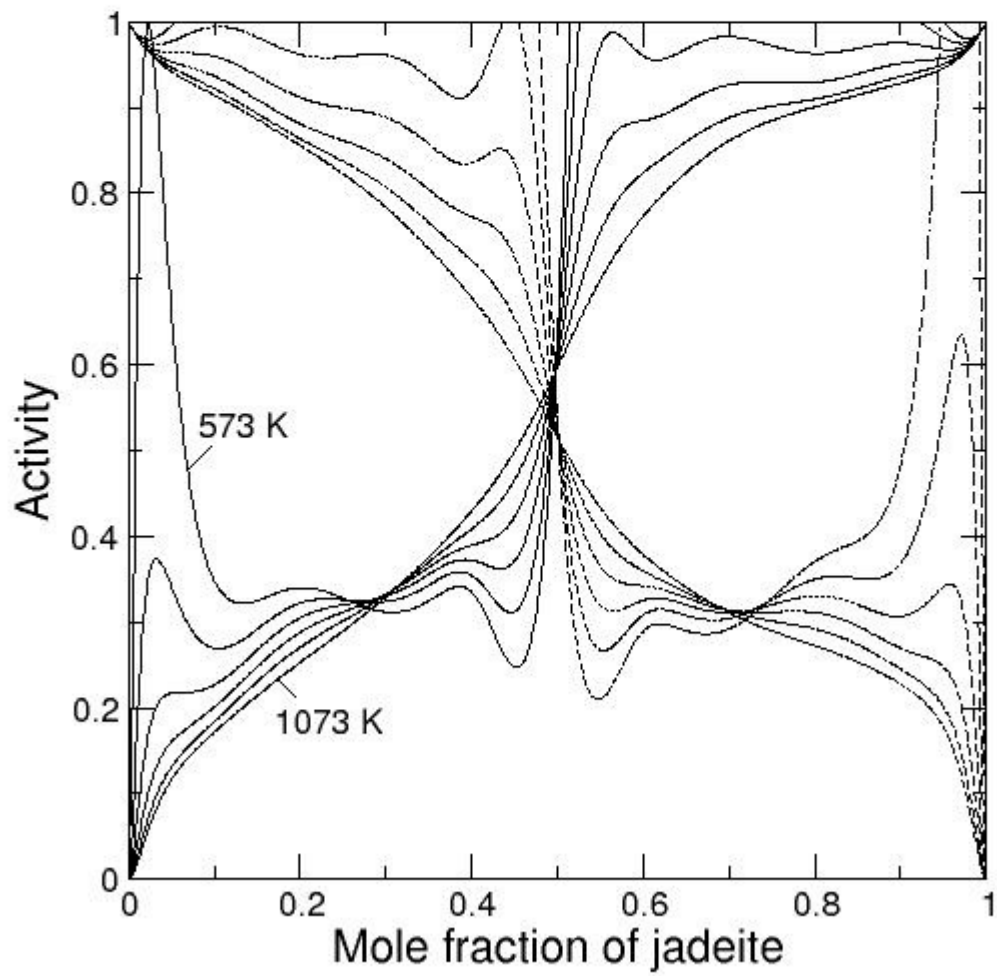
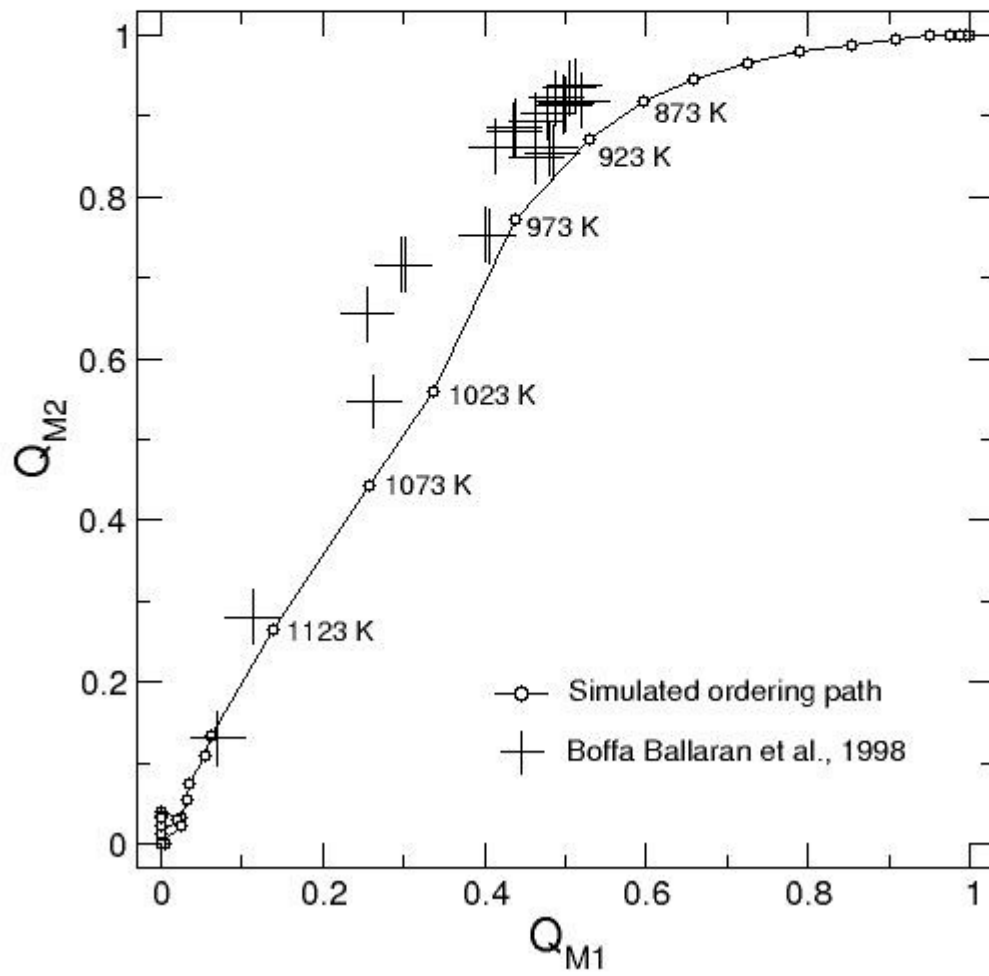Figure 5
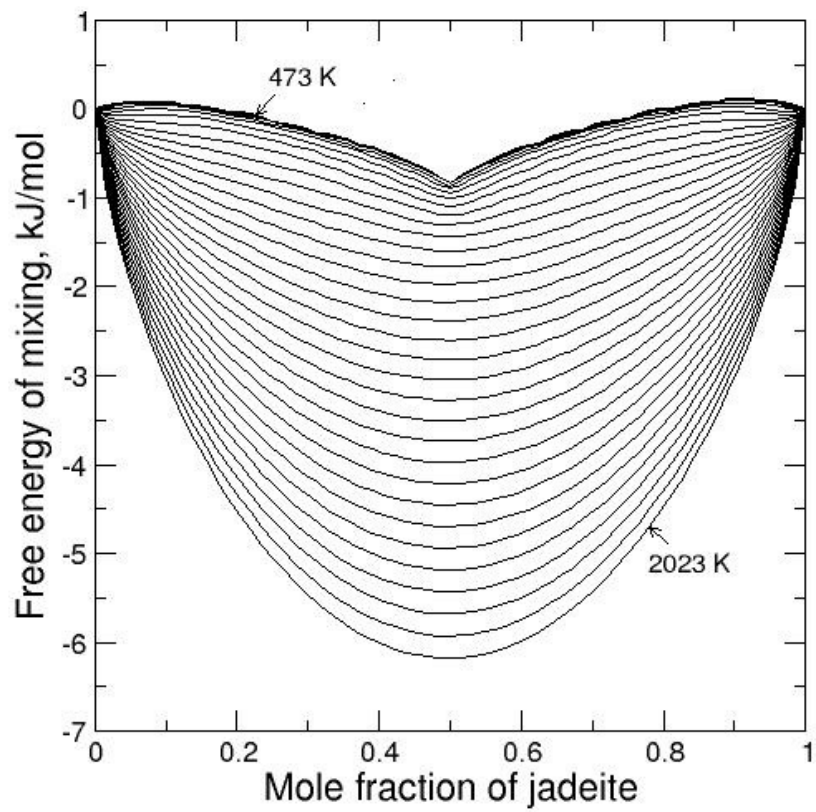
Figure 6
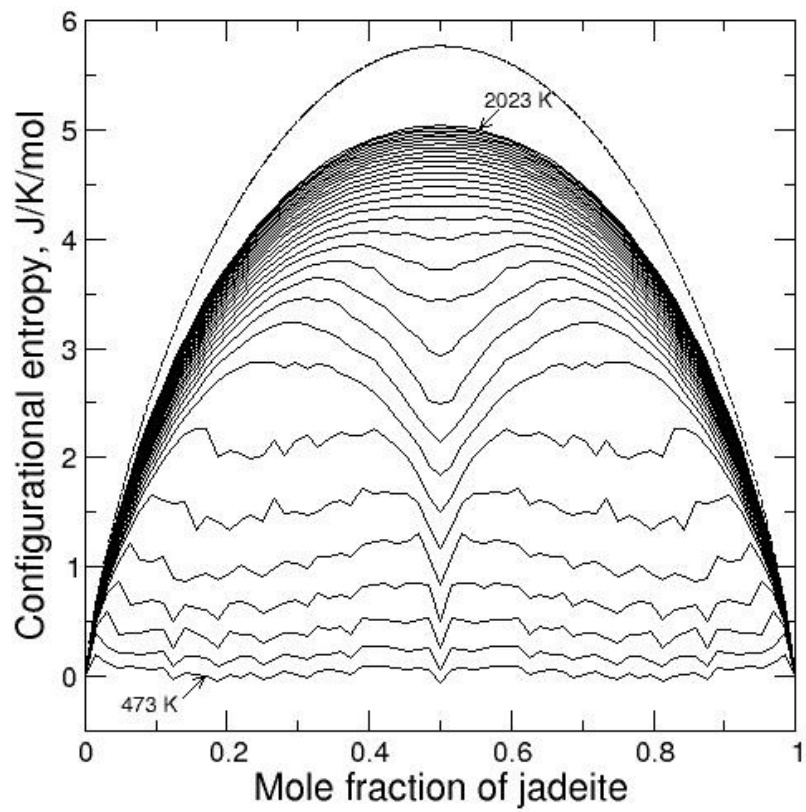
Figure 7
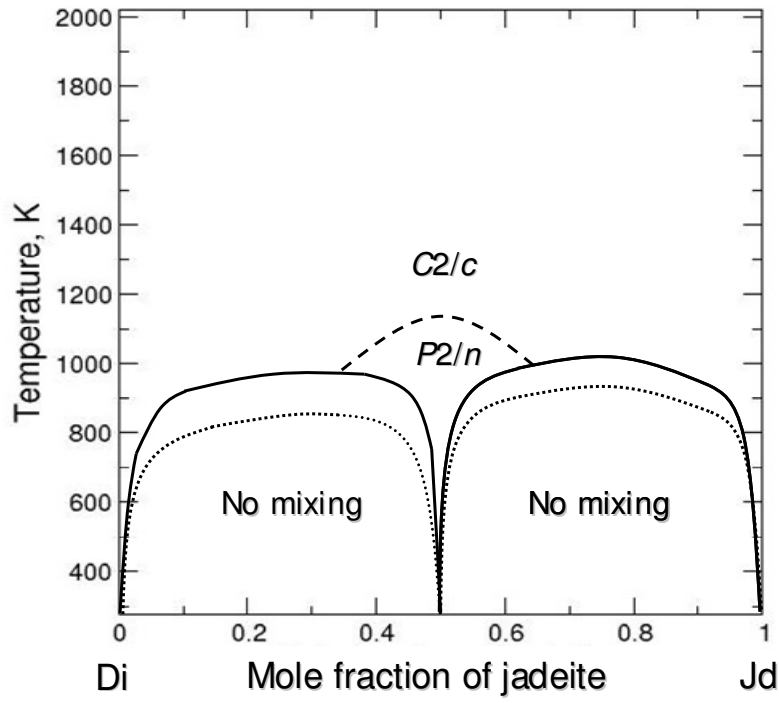
Figure 8
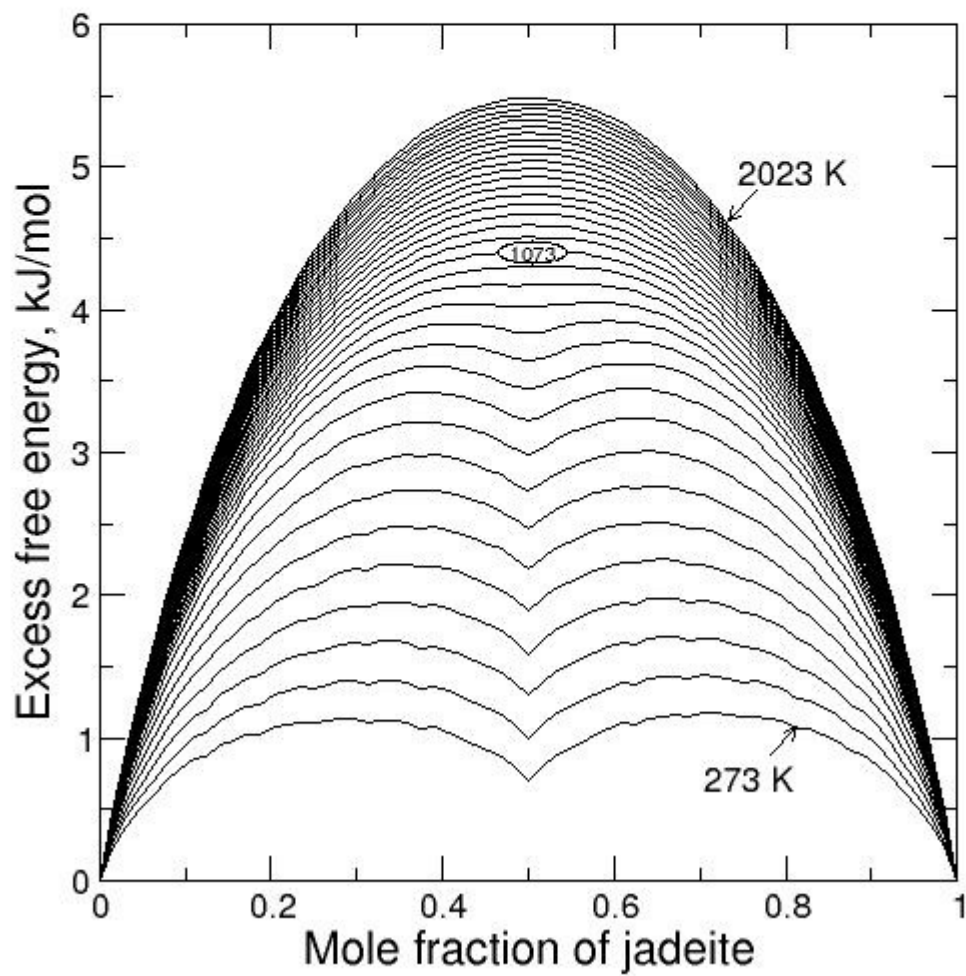
Figure 9.

Figure 10

Figure 11.

Figure 12

Figure 13

Figure 14